

GaN grown in polar and non-polar directions

Z. LILIENTAL-WEBER*, J. JASINSKI, and D.N. ZAKHAROV

Lawrence Berkeley National Laboratory, 62/203, Berkeley, CA 94720, USA

In this paper, defects formed in GaN grown by different methods are reviewed. Thin GaN films were grown on c-, m-, and a-planes on a number of substrates and typical defects as characterized by transmission electron microscopy are described. For polar epilayers grown on c-plane sapphire the typical defects are dislocations (edge, screw and mixed). The lowest dislocation density was obtained for homoepitaxial growth using molecular beam epitaxy (MBE) or hydride vapour phase epitaxy (HVPE). In these cases, the core structure of screw dislocations were studied in detail. In both cases, the cores are full. In the layers grown by HVPE the dislocations are decorated by pinholes stacked on top of each other. These pinholes are empty inside and their formation is attributed to impurities (oxygen) present in these layers. In these layers Ga-rich cores have been found. These were not observed in the layers grown by MBE on the top of the HVPE templates.

Epilayers grown in non-polar directions (m- or a-plane) have a high density of planar defects (stacking faults) terminated by partial dislocations. Only low energy faults were found. The majority of these faults are formed at the interface with the substrate and propagate to the sample surface.

Keywords: GaN films, MBE growth, HVPE, dislocations, polar and non-polar growth.

1. Introduction

The importance of III-V nitride compounds for blue and ultraviolet optoelectronics was recognized more than 30 years ago [1]. The delay in achieving commercial successes was caused by the lack of bulk GaN or structurally and thermally compatible hetero-substrates and by the difficulty of p-doping. The technical breakthroughs by Yoshida *et al.* [2], Akasaki *et al.* [3,4], and Nakamura *et al.* [5,6] have brought an acceleration in the progress of blue and ultraviolet light emitting diodes (LEDs) and lasers (LEDs) and other devices [5–7]. Because of the lack of lattice matched substrates, GaN is grown mostly on Al₂O₃ or SiC which have a 14% or 3.5% lattice mismatch, respectively. The growth of high quality epitaxial GaN on sapphire involves a number of key processing stages, the parameters of which have been determined largely empirically in recent years. The growth of buffer layer of AlN or GaN at a temperature well below the regular GaN growth temperature leads to a substantial improvement in the quality of GaN grown on top of such a buffer layer. Advances in GaN growth have been achieved using mostly metal-organic chemical vapour deposition (MOCVD) and hydride vapour phase epitaxy (HVPE). Molecular beam epitaxy (MBE) is also a suitable technique for the fabrication of high quality device structures using III-V nitrides due to the precise control of atomic order, thickness, interface abruptness and composition but its relatively low growth rate compared to

other techniques means that this technique is used only for special applications.

It was shown theoretically [8] and proven experimentally [9] that spontaneous and piezoelectric (induced) polarization are present within GaN-based active layers when this material is grown on (0001) Al₂O₃ or 6H-SiC. The total polarization aligned along [0001] direction of hexagonal GaN structure leads to high interface charge densities and spatial separation of the electron and hole wave function in quantum well structures, which alters the optoelectronic properties of devices. One possible solution to eliminate these effects is to grow GaN-based layers in nonpolar orientations, such as {1100} (m-plane) or {1120} (a-plane). In this paper, structural quality of GaN grown on c-, m- and a-plane will be compared. For growth on c-plane some structural differences will be discussed when using different growth methods such as MOCVD, HVPE, and MBE. Core structures of screw dislocations in GaN grown by HVPE layers and these grown by MBE on a GaN template (earlier grown by HVPE) will be compared.

2. Defects in GaN grown on sapphire c-plane

The growth of GaN on sapphire (Al₂O₃) by MOCVD usually starts as islands which eventually coalesce to form a continuous layer [10]. Many dislocation half-loops are observed in the buffer layer and in the main layer in the area just above the buffer. The density of these dislocations decreases when the layer is grown to greater thickness. The main defects observed in such layers are dislocations. Their density reaches the range of 10⁹–10¹⁰ cm⁻² in the area close

* e-mail: z_liliental-weber@lbl.gov

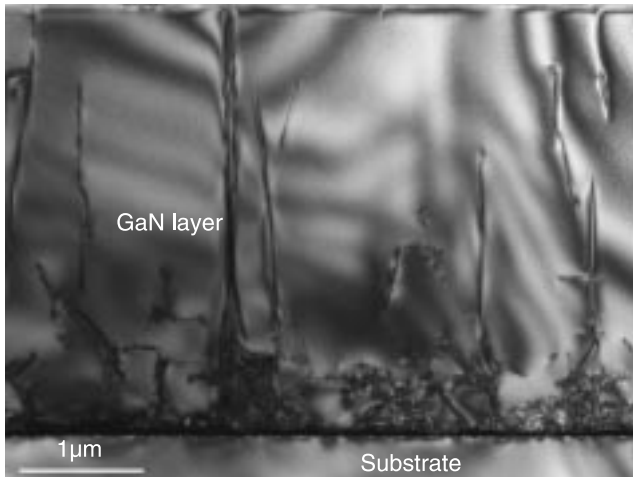


Fig. 1. A typical distribution of dislocations in the GaN cross-section sample grown by MOCVD.

to the buffer layer. Such a high density of these defects is detrimental for device applications. The work of Nakamura [11] showed that long lifetime laser diodes were achieved only for material where lateral overgrowth was applied, which is the method which substantially helped to decrease the number of dislocations in GaN material. The latest samples grown by this method show low dislocation den-

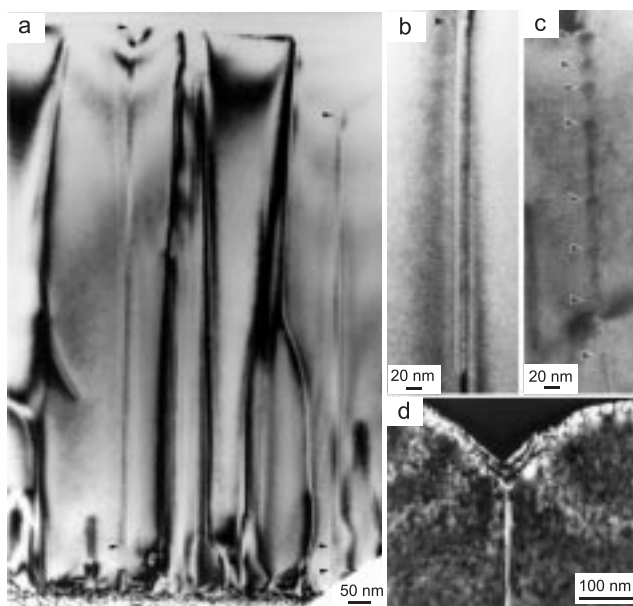


Fig. 2. (a) Defects (nanotubes, indicated by arrows, and dislocations) in a GaN layer grown on SiC by MOCVD with Ga polarity. Note that nanotube on the left hand-side propagates to the sample's surface and the one on the right hand-side is terminated inside the layer; (b) a nanotube along a screw dislocation terminated inside the GaN layer grown on SiO₂. A nanotube starts from a V-shape defect and then elongates in the c-direction with walls on (1100) planes; (c) pinholes with V-shape stacked on top of each other along a screw dislocation found in the MOCVD GaN layer grown on an Al₂O₃ substrate; (d) a pinhole attached to a screw dislocation formed at the surface of the same GaN layer.

sity ($\sim 2 \times 10^8 \text{ cm}^{-2}$) when the layer is about 3.5 μm thick (Fig. 1). In order to control defect formation, it is essential to understand the mechanisms of formation and the detailed structure of particular defects.

The majority of dislocations in GaN grown on c-plane sapphire using MOCVD are edge type with Burgers vectors at 90° to the c-axis. Transmission electron microscopy has shown that besides dislocations other defects are also formed such as nanotubes, pinholes and, occasionally, inversion domains [Figs. 2(a,b,c,d)].

It was observed that pinholes and nanotubes start from a V-defect [Fig. 2(a,b,c,d)] formed on (10 $\bar{1}$ 1) planes with about 56° between the V arms [see Fig. 2(d)], but only some of them develop into long empty tubes which either extend to the sample surface or terminate within the layer [Fig. 2(a,b)]. Both types of defects appear to have the same origin, a nanotube may develop from what is originally a pinhole and extend for long distances along the c-axis. Nanotubes and some pinholes are usually found along screw dislocations; some researches call such defects open screw dislocations.

It was proposed by Frank [12] that the minimum free energy for a dislocation of large Burgers vector would be achieved if its core were empty compared to a core filled with a highly strained lattice. According to Frank, the total energy is minimized when the radius "r" of an empty core

$$r = \mu b^2 / 8\pi^2 \gamma, \quad (1)$$

where \mathbf{b} is the Burgers vector of the dislocation, μ is the shear modulus, γ is the specific surface energy. However, this model does not fit the experimental observations [13]. The radii of the nanotubes have values ranging from a minimum at about 10 nm. From Eq. (1) it can be estimated that the Burgers vector \mathbf{b} corresponding to an empty tube of 10 nm should be 4 nm, which is an order of magnitude larger than the Burgers vectors observed in these experiments. Therefore, the Frank equilibrium model can hardly explain the presence of these empty holes. In addition, almost all tubes are closing inside the layer. This would cost additional energy. Therefore it would be difficult to consider that such action would take place. Our work has shown that formation of nanotubes could be related to impurities such as oxygen [13]. This was confirmed by recent studies of Arslan and Downing [14], but these authors call these defects open screw dislocations since these defects observed from the sample surface represent holes. These authors did not study these empty defects in cross-section configuration. Pinholes are often observed in the MOCVD grown GaN samples. In the majority of cases these defects are observed in the subsurface areas, but often these defects can be observed decorating a screw dislocation stuck on top of each other. These defects will be described in one of the following paragraphs.

In order to obtain information about dislocation core structures, high-resolution focal series were used together with a numerical reconstruction procedure to reconstitute

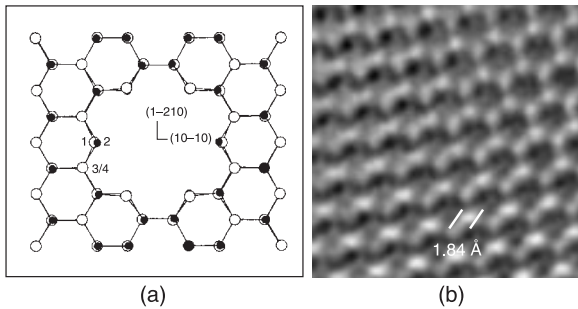


Fig. 3. (a) Model of open core screw dislocation (after Ref. 17). (b) Full core of screw dislocation in Ga-rich MBE grown GaN (all atomic columns are visible). Lack of difference in atomic column intensity between centre image and surrounding matrix indicates stoichiometric cores.

the electron wave at the specimen exit surface. To obtain structural information at higher resolution, 20 micrographs were obtained from each screw dislocation at large values of defocus and the complex electron wave function was reconstructed numerically. This method allows one to distinguish atomic columns separated from each other at least by 0.8 \AA [15,16]. In order to learn if a dislocation has full or open core, we investigated for missing atomic columns expected for the empty core as predicted theoretically [17] and shown in Fig. 3(a). We evaluated changes in intensity of particular columns or any indication of change from white to black atomic columns which would be expected for nonstoichiometric core for particular sample thickness and tilt as predicted by our calculations [18].

For this particular study screw dislocations in GaN grown by MBE from excess of Ga were considered. There were no pinholes or nanotube along such dislocations. Theoretical calculations were applied in order to understand how the reconstructed image would change when sample tilt or stoichiometry change would take place [18]. Our studies showed that screw dislocations in these MBE grown layers have a full core without a change of stoichiometry since all columns are visible without any change of intensity [the dislocation core is in the center of Figs. 3(b)].

TEM studies of HVPE grown material shows a high number of pinholes (voids) seen in cross-sectioned samples as triangles aligned along screw dislocations, forming a bamboo-like structure [Fig. 4(a)]. These voids are not distributed uniformly on each screw dislocation. In the area close to the sapphire substrate the density of these voids (pinholes) is much higher. Further from the substrate the density of these pinholes is much smaller. In a very thick HVPE layer, as shown in Fig. 4(b), the density is even lower. For GaN grown by MOCVD on such templates no decoration of screw dislocation was observed. Figure 4(b) shows the screw dislocation in the thick HVPE template overgrown by the MOCVD layer. The interface area between the same material grown by different techniques is shown. The pinholes (marked by arrows) appear only in HVPE layer, but not in the one grown by MOCVD. It is expected that layers grown by MBE (also by MOCVD) methods are much cleaner in comparison to the

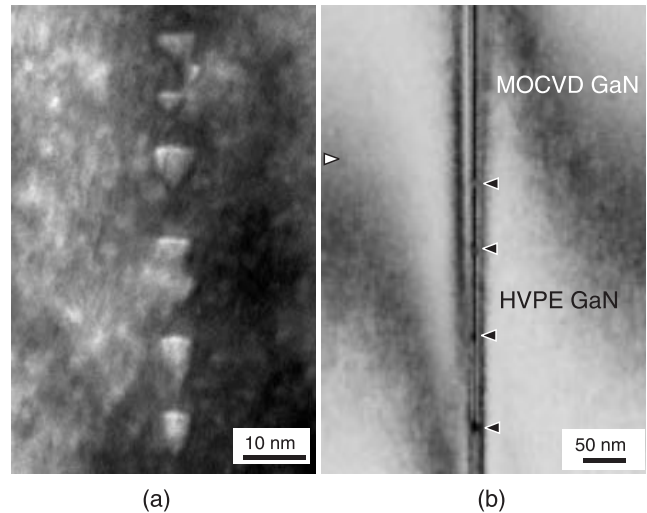


Fig. 4. (a) Pinholes along a screw dislocation in a HVPE GaN layer. Contrast on the dislocation disappears for this diffraction condition; (b) pinholes along a screw dislocation in the HVPE layer and lack of them in the layer grown on top of it by the MOCVD method. The image is taken with a diffraction condition for which the screw dislocation is in contrast.

HVPE grown samples and that these pinholes are due to impurities present there.

As mentioned earlier such dislocations with pinholes are called by other researchers open core dislocations [14]. In order to check if dislocations decorated by pinholes have open core they were studied in plan-view configuration using high-resolution focal series together with a numerical reconstruction procedure to reconstitute the electron wave at the specimen exit surface [15]. Since 20 micrographs necessary for the reconstruction were taken with different defocus close to the resolution limit of the microscope (using constant defocus step) different depth of sample was imaged, reaching the tip of the pinhole. In plan-view configuration these voids had a hexagonal shape [Fig. 5(a)] and reconstructions were obtained for [0001] projection where atomic columns are separated by 1.84 \AA [Figs. 5(b,c,d)]. In the dislocation core, one atomic column at the expected tip of the V-type defect was very weak [Fig. 6(a) – area A] and another column in the dislocation core is very bright [Fig. 6(a) – area B)]. Our calculations show [18] that weaker or stronger intensity of such columns cannot be obtained simply by sample tilt, therefore such a difference in their intensity can be assigned only to the stoichiometry of the particular column. Weaker intensity at the tip of the V-defect confirms our earlier suggestion that these defects are due to impurity accumulation on the low growth $(10\bar{1}1)$ planes [13]. No indication of a continuous hollow core screw dislocation was obtained based on this study.

Growth of GaN using HVPE is much faster than the growth using the MOCVD method, therefore, greater layer thickness can be grown in shorter time. By growing thicker layers more interactions between dislocations can take place, which leads to a smaller density of dislocations near the top surface. Interaction between dislocations takes

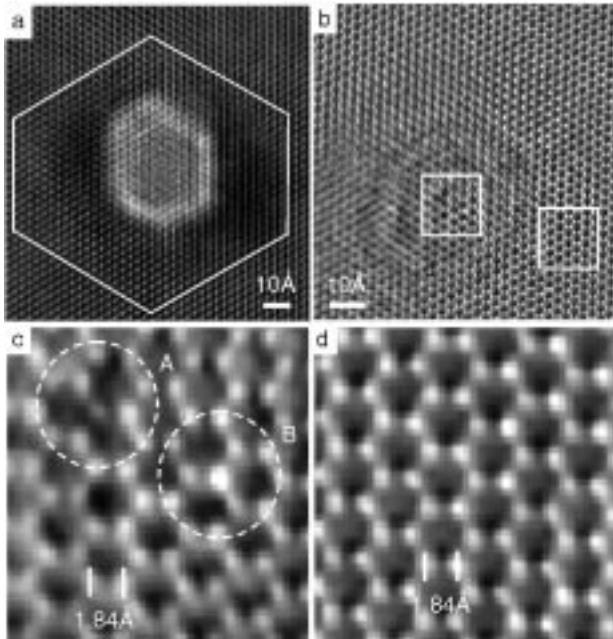


Fig. 5. (a) Burgers circuits around a screw dislocation from the HVPE grown GaN layer; (b) phase of the electron wave reconstruction from the screw dislocation surrounded by a void; (c) larger magnification of defect area outlined by a square. The reconstruction from the area around the tip of the void is marked by the circuit A and around the dislocation core by the circuit B. (d) Reconstruction in the perfect material. Note that all atomic columns in the vicinity of dislocation core shown in (c) are preserved (as in the perfect material) suggesting that a hollow dislocation core is not formed. The intensity of atomic columns is weaker in the vicinity of the tip of the V-shape void suggesting light elements present in the column.

place at the greatest rate in the area close to the interface with the substrate where more dislocations with inclined line directions to the *c*-axis are present. As the layer becomes thicker there are fewer interactions between dislocations since they are further apart and decrease in dislocation density becomes more difficult. Our studies showed that for layer thickness up to 300 μm , the dislocation density has an inverse proportionality to film thickness (Fig. 7) [19]. Such thick layers can be removed from the substrate and can serve as free-standing substrates. The lowest dislocation density obtained in the HVPE thick layers was $\sim 2 \times 10^6 \text{ cm}^{-2}$ [20].

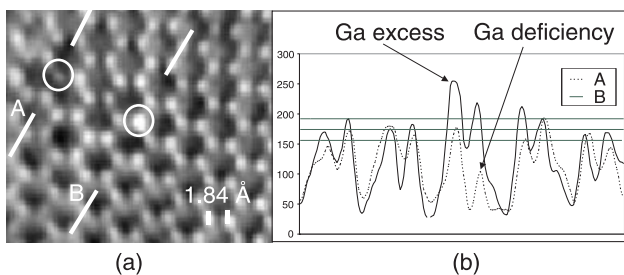


Fig. 6. (a) Image reconstruction of screw dislocation in HVPE sample. (b) Intensity profiles show reduced (A) and enhanced (B) image intensity, indicating Ga excess and deficiency.

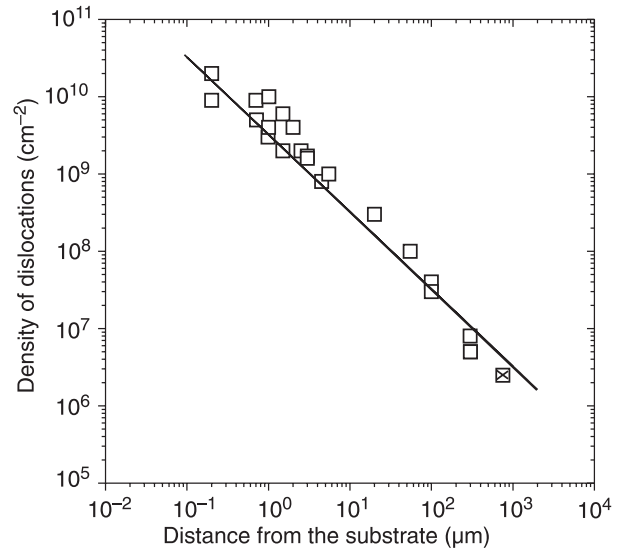


Fig. 7. Dependence of dislocation density on the layer thickness in the GaN grown by HVPE [after Ref. 19].

3. Growth of homoepitaxial GaN layers

For the growth of homoepitaxial layers bulk GaN grown from a solution of atomic nitrogen in liquid gallium under high nitrogen pressure (up to 20 kbars) in the temperature range 1500–1800 K have been used [21]. These bulk crystals crystallize with a wurtzite structure in the form of platelets which have the shape of elongated hexagons [22] where the longest axis is usually along [1120] and the shortest along [0001] perpendicular to the largest surface. The ratio of plate length to thickness along the *c* axis is typically about 100 showing that growth in the *c* axis direction is the most difficult. The largest platelets have a size close to 1 cm. These crystals are polar and the growth polarity influences the surface morphology. The surface of the plate with N polarity has a smooth surface while the opposite side is rough (Fig. 8). For the growth with N polarity, as-grown crystals can be used after careful cleaning but for the growth with Ga polarity bulk crystals are first mechanically polished followed by reactive ion etching.

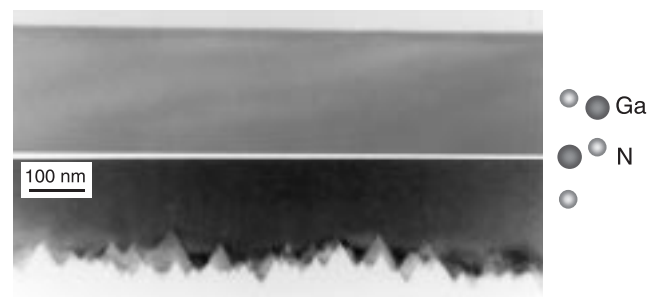


Fig. 8. A cross-section micrograph through a bulk GaN platelet showing the different surface roughness for opposite growth polarity (indicated on the right). High densities of planar defects (stacking faults and dislocation loops decorated by Ga precipitates) were found near the rough side of the platelet.

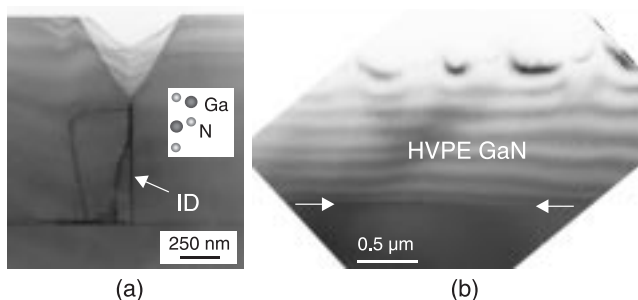


Fig. 9. (a) An inversion domain (ID) with a pinhole formed on top of it and a threading dislocation attracted to the pinhole formed in a MOCVD GaN layer grown with N-polarity on a bulk GaN substrate. All these defects started from the dislocation loop (darker contrast observed at the interface). A continuous dark line at the interface between the substrate and the epilayer indicates the presence of some types of inhomogeneity; (b) GaN layer grown also with N-polarity by HVPE on a bulk GaN substrate, first polished and etched by reactive ion etching (b).

TEM studies of the samples grown directly on bulk GaN platelets without a buffer layer showed that MOCVD epitaxial layers retain the polarity of the substrate [23]. However, growth on the two opposite *c*-surfaces (different polarity) is not equivalent from the point of view of defects in the homoepitaxial layers. In the epi-layer grown on the N-polar surfaces threading dislocations and inversion domains were found [Fig. 9(a)]. These threading dislocations started either from dislocation loops formed at the interface or from some small “surface disturbances” from which several threading dislocations originated. Pinholes with walls on (10 $\bar{1}$ 1) planes at the top of inversion domains were also observed. Since in this case growth is forced to be along the *c*-axis, which is much slower than growth in the perpendicular

direction, impurities have enough time to accumulate on (10 $\bar{1}$ 1) polar planes. It has been found that the N-polar surface decomposes faster and initiation of the growth has to be done at lower temperature than in the case of growth with Ga-polarity. This may explain why dislocation loops were formed at the interface which resulted in the formation of threading dislocations and inversion domains.

For the layer grown on the rough surface (Ga-polarity) no threading dislocations were observed. The interface between the substrate and the layer was not easily visible suggesting a very good continuation of growth in the layer [23]. However, a high density of pinholes ($\sim 10^6$ – 10^7 cm $^{-2}$) was observed.

Such bulk GaN substrates were also used as substrates for the growth of GaN layers by the HVPE technique [24]. No threading dislocations were present in these layers. The big difference was in the growth rate for the two polarities and in the surface smoothness. Growth with Ga polarity was three times faster than growth with N polarity, however, in the later case the surface was more smooth [Fig. 9(b)]. Formation of some dislocation loops for growth with N polarity was observed, as was the case for growth using the MOCVD technique.

4. Growth of *m*-plane GaN(1 $\bar{1}$ 00) on γ -LiAlO $_2$ (100) substrate

Growth of GaN on γ -LiAlO $_2$ (tetragonal crystal structure) attracted significant attention since its (100) face is closely matched to the (10 $\bar{1}$ 0) face (*m*-plane) of wurtzite GaN. Lattice mismatch of -1.4% is expected along the *c*-axis ($[001]_{\text{LiAlO}_2} \parallel [12\bar{1}0]_{\text{GaN}}$) and of -0.1% only along the *b*-axis of γ -LiAlO $_2$ ($[010]_{\text{LiAlO}_2} \parallel [0001]_{\text{GaN}}$). GaN devices

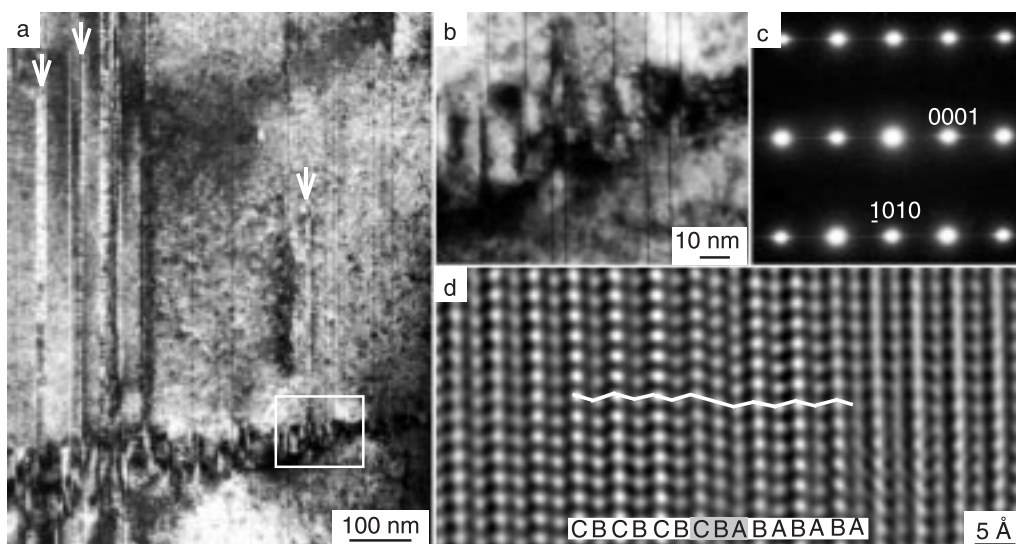


Fig. 10. (a) Dark-field image of cross-sectional sample taken with diffraction vector $g = (0001)$. Majority of thin lines are SFs but these ones indicated by white arrows are thin domains. (b) Enlargement of the area marked by the rectangular frame in (a) showing basal stacking faults as narrow dark lines. Some of them terminate and some nucleate at the inclined boundary. (c) Selected area electron diffraction pattern obtained from the image shown in (a) with diffraction spot streaking in the [0001] direction; (d) high resolution image of a I_1 basal stacking fault.

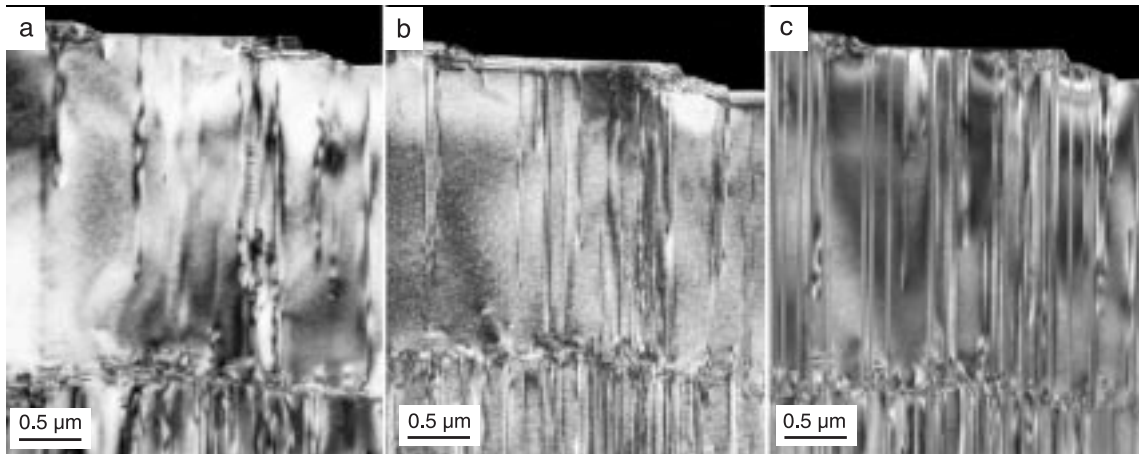


Fig. 11. Dark-field TEM images of the sample area showing dislocations in cross-sectional specimen imaged with different diffraction condition to determine their nature (a) $g = (0002)$, (b) $g = (1120)$, and (c) $g = (1010)$.

grown with the m-plane show lack of spontaneous electrostatic fields along the growth direction [25,26]. It has also been shown that the peak position of emission from the GaN/AlGaIn multi-quantum well structures grown on c-plane is strongly blue shifted with increasing excitation intensity, whereas the peak position for m-plane structures remains unchanged [27]. TEM studies of the (1010) GaN grown on γ -LiAlO₂ show that despite the apparent good lattice match with the substrate high densities of structural defects are formed in GaN layers [28]. Several types of structural defects were observed, such as stacking faults (SFs) and other planar defects formed on the basal plane, some boundaries located on prism planes and threading dislocations. Since c-planes are perpendicular to the substrate, SFs formed on these planes are visible on cross-section micrographs as straight lines [Fig. 10(a,b)] since these defects are in edge-on configuration. High resolution image of these faults reveals I_1 type of the fault

which changes AB atomic stacking configuration to CB and this configuration within the fault area can be described as ABABABCBCB [Fig. 10(d)], where each capital letter represents a bi-atomic, Ga-N layer. This is a fault with the lowest formation energy among three different types of faults present in wurtzite structure. It is equivalent to the insertion of one cubic unit within the wurtzite structure. This fault is formed by the removal of a basal layer followed by the slip of one part of the crystal by $1/3[10\bar{1}0]$. Diffraction pattern in Fig. 10(c) shows the streaking along [0001] from a high number of basal stacking faults.

The boundary which is shown in Figs. 10(a) and 10(b) is located on a prism plane inclined to the growth plane and plays a role of termination or nucleation of SFs. Besides the planar defects threading dislocations are also present in these layers [Figs. 11 (a,b,c)]. The density of these dislocations decreased from the value of 10^9 cm^{-2} close to the substrate to the 10^8 cm^{-2} at the layer surface.

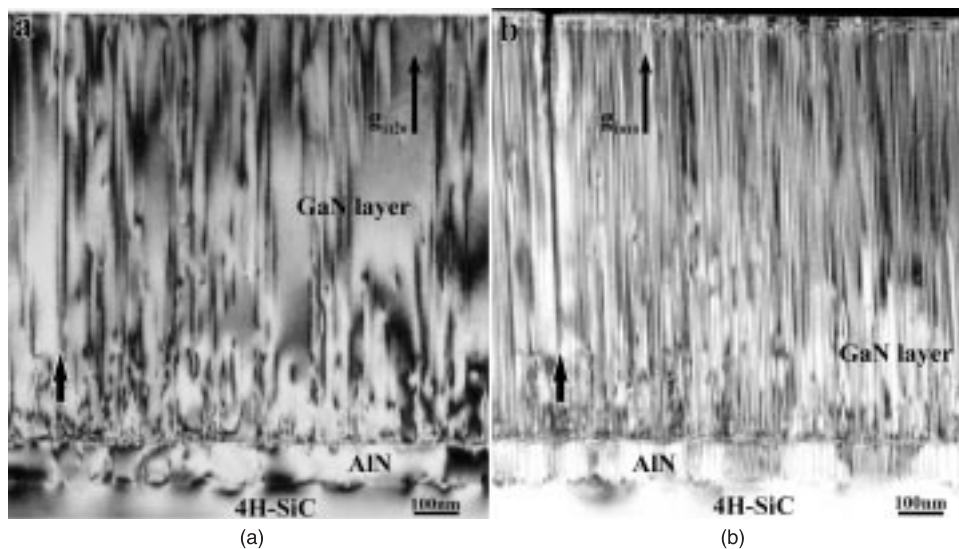


Fig. 12. (a) Bright field image of cross-section GaN sample taken with $g = (1120)$ showing dislocations with the component of Burgers vector parallel to $[1120]$; (b) Dark field image taken with $g = (1010)$ showing nucleation of stacking faults at the AlN/4H SiC interface. These faults propagate to the sample surface. A crack (marked by arrow) is formed in this sample.

5. Growth of a-plane GaN on 4H-SiC

Growth of $\{11\bar{2}0\}$ (a-plane) GaN can be archived by using 4H-SiC substrate with the AlN buffer layer. Such layers demonstrate polarization free behaviour along the growth direction. TEM studies of these layers show high density of stacking faults [Figs. 12(a,b)] and threading dislocations [25,29]. Orientation relationship between the substrate and the layer can be written as follows: $(11\bar{2}0)\text{GaN} \parallel (11\bar{2}0)\text{AlN} \parallel (11\bar{2}0)\text{4H-SiC}$ and $[1\bar{1}00]\text{GaN} \parallel [1\bar{1}00]\text{AlN} \parallel [1\bar{1}00]\text{4H-SiC}$. The majority of these faults are also low energy stacking faults I_1 , as described in the previous paragraph. Frank partial dislocations with $b = 1/3[10\bar{1}0]$ and $b = 1/3[01\bar{1}0]$ terminating these faults are shown in plan-view configuration [Figs. 13(a,b)]. Density of partial dislocations terminating I_1 stacking fault is $\sim 4 \times 10^{10} \text{ cm}^{-2}$.

Majority of these basal stacking faults nucleated at the substrate/AlN buffer layer interfaces and only some in GaN. Some of them terminated within the GaN layer but most of them continued through the entire layer. In some areas also I_2 stacking faults with atomic sequence ABABABCACAC with higher formation energy than I_1 type of faults were also formed. These faults can be formed either by shear of crystal in a basal plane by $1/3\langle 1100 \rangle$ or by dissociation of perfect dislocation into two Shockley partials with $b = 1/3\langle 1100 \rangle$. These faults were expected to be formed as a result of local stress relaxation arising in c-plane from lattice mismatch and different thermal expansion coefficients.

6. Conclusions

This review of defects in GaN grown on different crystallographic planes show that in each case density of defects is high for layers grown heteroepitaxially. For MOCVD layers grown on c-plane (on Al_2O_3 or SiC) Ga growth polarity can be determined. High density of dislocations (edge, screw and mixed) are formed. These defects can be reduced by growing

layers with larger thickness (such as observed for the growth by HVPE method) to take advantage of interaction between dislocations, especially in the areas close to the buffer layer where dislocation density is high, and they are closely spaced. Lateral epitaxial overgrowth can be also used to allow bending of dislocations over SiO_2 masks deposited on highly defective GaN layer [30–32]. The density of dislocations is by far the lowest when GaN is grown homoepitaxially. Growth with HVPE on bulk crystals is very promising, for both N- and Ga-growth polarity. Defect density in such layers is negligible. Full core structure of screw dislocations in the layers grown by MBE and HVPE was observed and these cores in the HVPE layers were Ga-rich. The screw dislocations in HVPE layers were decorated by pinholes.

Growth of m- or a-plane GaN is non-polar; therefore problems related to spontaneous and induced polarization are not present. However, in both type of samples a high density of stacking faults was observed independently from substrate used ($\gamma\text{-LiAlO}_2$ or 4H-SiC). In both these cases c-plane of GaN is along growth direction and stacking faults are formed on these planes since their formation energy is very low. Most of these faults start from the interface with the substrate. They propagate to the sample surface since growth direction $[11\bar{2}0]$ or $[1\bar{1}00]$ is faster than growth along $[0001]$. It is believed that in order to utilize materials grown on m- or a-planes for devices lateral overgrowth or other method which leads to decreasing defect density need to be applied.

Acknowledgments

This work was supported by the U.S. Department of Energy under the contract No. DE-AC03-76SF00098. The use of the facility at the National Centre for Electron Microscopy at the LBNL is greatly appreciated. The authors want to thank Drs. S. Porowski, I. Grzegory, J. Baranowski, R. Dupuis, R. Molnar, H. Morkoc and S.S. Park for providing GaN samples.

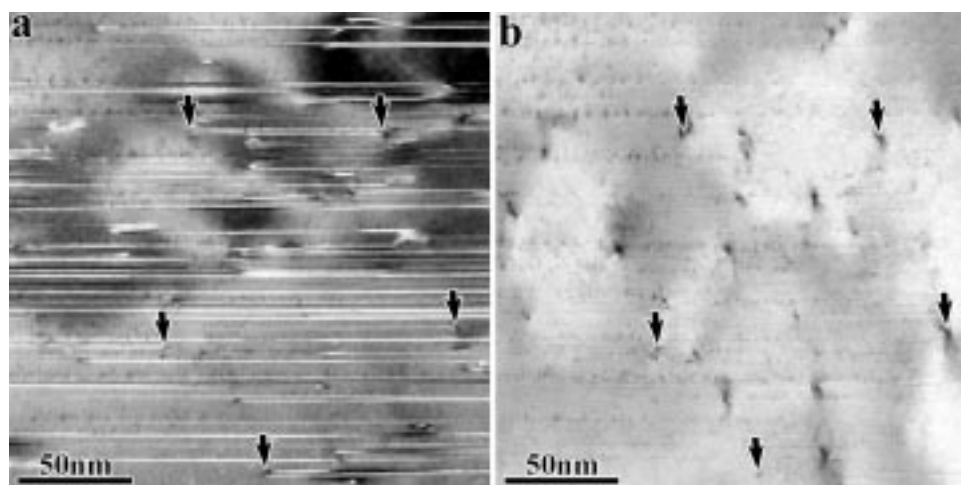


Fig. 13. TEM bright field image of plan-view sample obtained with two perpendicular diffraction condition (a) $g = (1100)$ where parallel lines indicate stacking faults formed on the basal plane of GaN; (b) 0002 where partial dislocations with Burgers vector $b = 1/6 [2\bar{2}03]$ are terminating stacking faults (the $[0001]$ component of the Burgers vector is in contrast). The arrows on both images show termination of stacking faults by partial dislocations.

References

1. J.I. Pankove, E.A. Miller, and J.E. Berkeyheiser, *RCA Rev.* **32**, 383 (1971).
2. S. Yoshida, S. Misawa, and S. Gonda, *J. Vac. Sci. Technol.* **B1**, 250 (1983).
3. H. Amano, N. Sawaki, I. Akasaki, and Y. Toyoda, *Appl. Phys. Lett.* **48**, 353 (1986).
4. I. Akasaki, H. Amano, M. Kito, and K. Hiramatsu, *J. Lumin.* **48/49**, 666 (1991).
5. S. Nakamura, M. Senoh, and T. Mukai, *J. Appl. Phys.* **30**, L1709 (1991).
6. S. Nakamura, M. Senoh, S. Nagahama, N. Iwasa, T. Yamada, T. Matsushida, Y. Sugimoto, and H. Kiyogu, *Appl. Phys. Lett.* **70**, 1417 (1997).
7. B.W. Lim, Q.C. Chen, J.Y. Yang, and M.A. Khan, *Appl. Phys. Lett.* **68**, 3761 (1996).
8. T. Nishida and N. Kobayashi, *Phys. Stat. Sol.* **A188**, 113 (2001).
9. F. Bernardini and V. Fiorentini, *Phys. Rev.* **B57**, 9427 (1998).
10. S. Ruvimov, Z. Liliental-Weber, H. Amano, and I. Akasaki, *MRS Proc.* **482**, 387 (1998).
11. S. Nakamura, M. Senoh, S. Nagahama, N. Iwasa, T. Yamada, T. Matsushita, H. Kikyoku, Y. Sugimoto, T. Kozaki, H. Umemoto, M. Sano, and K. Chocho, *Jap. J. Appl. Phys.* **36**, L1568 (1997).
12. F.C. Frank, *Acta Cryst.* **4**, 497 (1951).
13. Z. Liliental-Weber, Y. Chen, S. Ruvimov, and J. Washburn, *Phys. Rev. Lett.* **79**, 2835 (1997).
14. I. Arslan and N.D. Browning, *Phys. Rev. Lett.* **91**, 165501 (2003).
15. A. Thust, W.M.J. Coene, M. Op De Beeck, and D. Van Dyck, *Ultramicroscopy* **64**, 211 (1996).
16. M.A. O'Keefe, E.C. Nelson, Y.C. Wang, and A. Thust, *Phil. Mag.* **B81**, 1861–1878, (2003).
17. J. Elsner, R. Jones, P.K. Sitch, V.D. Porezag, M. Elstner, Th. Frauenheim, M.I. Heggie, S. Öberg, and P.R. Briddon, *Phys. Rev. Lett.* **79**, 3672 (1997).
18. Z. Liliental-Weber, D. Zakharov, J. Jasinski, M.A. O'Keefe, and H. Morkoc, *Microscopy and Microanalysis* **10**, 47–54, (2004).
19. J. Jasinski and Z. Liliental-Weber, *J. Electr. Mat.* **31**, 429 (2002).
20. D.C. Look, J.R. Sizelove, J. Jasinski, Z. Liliental-Weber, K. Saarinen, S.S. Park and J.H. Han, *Mat. Res. Symp. Proc.* **743**, L10.1.1 (2003).
21. I. Grzegory, J. Jun, M. Bockowski, St. Krukowski, M. Wroblewski, B. Lucznik, and S. Porowski, *J. Phys. Chem. Solids* **56**, 639 (1995).
22. Z. Liliental-Weber, C. Kisielowski, S. Ruvimov, Y. Chen, J. Washburn, I. Grzegory, M. Bockowski, J. Jun, and S. Porowski, *J. Electr. Mat.* **25**, 1545 (1996).
23. J.M. Baranowski, Z. Liliental-Weber, K. Korona, K. Pakula, R. Stepniewski, A. Wyszomolek, I. Grzegory, G. Novak, S. Porowski, B. Monemar, and P. Bergman, *Mater. Res. Soc. Symp.* **449**, 393 (1997).
24. Z. Liliental-Weber, J. Jasinski, and J. Washburn, *J. Cryst. Growth* **246**, 259–270 (2002).
25. P. Waltereit, O. Brandt, M. Ramsteiner, A. Trampert, H.T. Grahn, J. Menniger, M. Reiche, R. Uecker, P. Reiche, K.H. Ploog, *Physica Status Solidi* **A180**, 133. (2000).
26. P. Waltereit, O. Brandt, A. Trampert, H.T. Grahn, J. Menniger, M. Ramsteiner, M. Reiche, and K.H. Ploog, *Nature* **406**, 865 (2000).
27. E. Kuokstis, C.Q. Chen, M.E. Gaevski, W.H. Sun, J.W. Yang, G. Simin, M. Asif Khan, H.P. Maruska, D.W. Hill, M.C. Chou, J.J. Gallagher, B. Chai, *Appl. Phys. Lett.* **81**, 4130 (2002).
28. J. Jasinski, Z. Liliental-Weber, H.P. Maruska, B.H. Chai, D.W. Hill, M.M.C. Chou, J.J. Gallagher, and S. Brown, *Mat. Res. Soc. Symp. Proc.* **764**, C6.6 (2003).
29. D.N. Zakharov, Z. Liliental-Weber, B. Wagner, Z.J. Reitmeier, E.A. Preble, and R.F. Davis, work in prep. for publ.
30. T.S. Zheleva, O.H. Nam, M.D. Bremser, and R.F. Davis, *Appl. Phys. Lett.* **71**, 2473 (1997).
31. D. Kaplonek, S. Keller, R. Ventury, R.D. Underwood, P. Kozodoy, S.P. Den Baars, and U.K. Mishra, *Appl. Phys. Lett.* **71**, 1204 (1997).
32. J. Park, P.A. Grudowski, C.J. Eitingm, and R.D. Dupuis, *Appl. Phys. Lett.* **73**, 333 (1998).